How unusual was Australia's 2017–2019 Tinderbox Drought?

Georgina Falster[1,2], Sloan Coats[3], Nerilie Abram[1,2,4]

[1]Research School of Earth Sciences, Australian National University, ACT, 2601 Canberra, Australia
[2]ARC Centre of Excellence for Climate Extremes, Australian National University, ACT, 2601 Canberra, Australia
[3]Department of Earth Sciences, University of Hawai'i at Mānoa
[4]Australian Centre for Excellence in Antarctic Science, Australian National University, ACT, 2601 Canberra, Australia

Correspondence to: Georgina M. Falster (georgina.falster@anu.edu.au)

This is a preprint (submitted to EarthArXiv) of a manuscript currently in review at Weather and Climate Extremes (as of 2024-09-19).

PREPRINT

How unusual was Australia's 2017–2019 Tinderbox Drought?

Georgina Falster[1,2], Sloan Coats[3], Nerilie Abram[1,2,4]

[1]Research School of Earth Sciences, Australian National University, ACT, 2601 Canberra, Australia
[2]ARC Centre of Excellence for Climate Extremes, Australian National University, ACT, 2601 Canberra, Australia
[3]Department of Earth Sciences, University of Hawai‘i at Mānoa
[4]Australian Centre for Excellence in Antarctic Science, Australian National University, ACT, 2601 Canberra, Australia

Correspondence to: Georgina M. Falster (georgina.falster@anu.edu.au)

Abstract

Australia's Murray-Darling Basin experienced three consecutive years of meteorological drought across 2017–2019, collectively named the 'Tinderbox Drought'. Rainfall deficits during the three-year drought were most pronounced in the Australian cool season (April to September). Deficits in both the cool season and annual total rainfall were unprecedented in the instrumental record. However, the instrumental record provides just one of a range of equally plausible climate trajectories that could have occurred during this period. To determine if the Tinderbox Drought was outside this range, we used observational data from prior to the onset of the drought to construct Linear Inverse Models (LIMs) that emulate the stationary statistics of Australian rainfall and its connection to global sea surface temperature (SST) anomalies. Overall, we find that rainfall deficits were most unusual in the northern Murray-Darling Basin, and during the final year of the drought. The global SST anomalies observed during the first two years of the Tinderbox Drought, particularly the cool anomalies in the central tropical Pacific and western Indian Ocean, are not typically associated with low rainfall across the Murray-Darling Basin. In terms of single-year rainfall anomalies, the only aspect of the Tinderbox Drought that was beyond the range of the LIMs was annual-total rainfall over the northern Murray-Darling Basin during 2019. This coincided with an extreme positive Indian Ocean Dipole event that was also beyond the range of the LIMs. When considered in terms of basin-wide rainfall over the full three years, rainfall deficits during the Tinderbox Drought were beyond the LIM range in terms of both cool-season and annual-total rainfall. This suggests an anthropogenic contribution to the severity of the drought—likely exacerbated by the 2019 extreme positive Indian Ocean Dipole event.

PREPRINT

1 Introduction

Australia's 2017–2019 'Tinderbox' Drought was unprecedented in the historical record. The drought was focussed over the Murray-Darling Basin (MDB) in southeast Australia (Fig. 1), and was characterized by an overall ~50% deficit in cool season (April to September) rainfall (Devanand et al., 2024), spanning the D'harawal seasons of Marrai'gang, Burrugin, and Wiritjiribin. The traditional lands of the First Nations D'harawal people span part of the south-eastern MDB, and the D'harawal people retain a deep understanding of the local climatology, developed over tens of thousands of years. Recognising this in turn provides deeper insights into how and where the Australian climate is changing (Lansbury et al., 2023).

The MDB is the largest agricultural region in Australia, and the Murray-Darling river system provides drinking water to many eastern Australian cities and towns. The sustained lack of rainfall during the Tinderbox Drought caused declines in evapotranspiration, streamflow and water storage (Devanand et al., 2024). The severity of the drought was further worsened by high air temperatures and high vapor pressure deficit (Devanand et al., 2024), ultimately setting the conditions for the 2019/2020 'Black Summer' fires and causing an estimated total national welfare loss of AU$63 billion (Wittwer and Waschik, 2021). Declines in river flow also had severe implications for the natural environment, for example mass fish death events across the MDB in 2018 and 2019 (Vertessy et al., 2019), including Guddhu (Murray cod) and Dhagaay (Murray perch)—both of which have important cultural value to First Nations people in the MDB.

MDB rainfall is expected to decline on average—and particularly during the cool season—due to human-caused climate change (Grose et al., 2020). Consistent with this, cool-season rainfall in south-eastern Australia has declined over past decades (BoM, 2022; McKay et al., 2023). Accordingly, First Nations people have observed changing river flow regimes, declining water quality, and changes in seasonality—with flow-on consequences for MDB biodiversity (Lansbury et al., 2023). However this rainfall decline is not yet unambiguously attributable to climate change (McKay et al., 2023). This lack of an attributable change is likely due to the MDB's high rainfall variability, which in turn is affected by a complicated network of local and remote drivers (McKay et al., 2023). These include large-scale modes of climate variability such as the El Niño Southern Oscillation (ENSO) and the Indian Ocean Dipole (IOD), as well as sea surface temperature (SST) anomalies in the tropical oceans north of Australia (Devanand et al., 2024; Nicholls, 2010; van Rensch et al., 2015). Despite the significant long-term association of historical MDB rainfall anomalies with ENSO variability, ENSO is unlikely to have been a major driver of rainfall deficits during the Tinderbox Drought (Devanand et al., 2024). Instead, cool SSTs in the eastern Indian Ocean (indicating positive IOD conditions) likely contributed to the deficits, especially during the final year of the drought that coincided with the strongest positive IOD event on record (Devanand et al., 2024).

Impacts of the Tinderbox Drought were particularly costly because a drought of equal or greater severity had not been experienced in the MDB since European water use and management began in Australia—despite that the MDB experienced longer but less severe historical droughts, such as the 1997–2009 Millennium Drought. Short, severe droughts pose different water management challenges to longer, less severe droughts (e.g., Stewart et al., 2020), such that historical experience was insufficient for both agricultural and water resource management agencies and community support networks to adequately anticipate and prepare for the Tinderbox Drought. To inform effective preparation for future droughts, it is important to quantify the full possible natural range of variability in MDB rainfall. We can then determine whether the Tinderbox Drought fell within the range of rainfall deficits that are possible from natural climate variability alone, or if human-caused climate change must have played a role in the drought's occurrence and/or severity.

The ~120 year instrumental record of Australian rainfall represents just one of a range of equally plausible climate histories that could have occurred during this period. Hence, the instrumental record is unlikely to have captured the full range of hydrological extremes that are possible from natural variability alone, particularly for multi-year events. That is, our available observations are an incomplete sampling of Australian rainfall variability (Falster et al., 2024) and thus it is impossible to determine whether the Tinderbox Drought was outside the *expected* range of variability using observations alone.

More complete records of Australian rainfall variability are available from climate model simulations of the pre-industrial past millennium (Falster et al., 2024), long unforced 'control' runs (Falster et al., 2024), and initial condition large ensembles (Mankin et al., 2020; Wood et al., 2021). The much greater number of years available in these simulations allows a long enough time for the most extreme hydrological conditions that are possible within these simulation frameworks to be characterized, and for small anthropogenic trends to be identified within the large natural variability of Australian rainfall. For example, comparison of the rainfall anomalies during the Tinderbox Drought with Australian rainfall simulated by Coupled Model Intercomparison Project (CMIP6) models suggest an ~18.4% anthropogenic contribution to observed cool-season rainfall deficits during the Tinderbox Drought (Devanand et al., 2024).

However, CMIP-class climate models have known biases and substantial intermodel spread in Australian rainfall (Grose et al., 2020; King et al., 2015) such that these climate model-based estimates must be tested with other data types. Natural archives of past rainfall variability such as tree rings, stalagmites, corals, ice cores and lake sediments—referred to as 'paleoclimate' records—are one such source, acting as proxies for direct observations. Paleoclimate data can potentially extend the length of the instrumental record by hundreds of years, sampling more of the full possible range of natural rainfall variability. Annually-resolved paleoclimate records with a strong mechanistic link to MDB rainfall can provide a valid comparison with rainfall during the three-year Tinderbox Drought, however such paleoclimate records are sparsely distributed in Australia. Instead, our present understanding of long-term rainfall variability in the MDB is based almost entirely on paleoclimate records from outside the MDB (Cook et al., 2016; Freund et al., 2017; Ho et al., 2015; Palmer et al., 2023; Vance et al., 2015). These remote records often have low correlations with MDB rainfall and require assumptions of stationary climate teleconnections over long periods of time, resulting in uncertainty in paleoclimate proxy-derived estimates of long-term rainfall variability and extremes in the MDB.

Here we use an alternate method to quantify the degree to which the Tinderbox Drought was unusual. We use instrumental observations of Australian rainfall and global SSTs to construct Linear Inverse Models (LIMs) that emulate the stationary statistics of Australian rainfall and its association with regional-to-large scale climate variability. By running the LIMs forced with noise we can produce long-term (many thousands of years) surrogate records of Australian rainfall variability. LIMs have been applied in other regions of the world to characterize the likelihood and causes of multi-year droughts, for example demonstrating that severe megadroughts known to have occurred in the western USA during the last millennium are also possible in today’s climate (Ault et al., 2018). Here, we apply the LIM approach to Australian multi-year droughts, and use this tool to answer the following question: Although MDB rainfall deficits during the Tinderbox Drought were unprecedented, was the intensity of this event foreseeable based on the characteristics and major drivers of Australian rainfall over the preceding century? We additionally seek to determine (a) the global surface ocean conditions most reliably associated with dry conditions in the MDB; and (b) whether the global surface ocean conditions during the Tinderbox Drought reliably bring dry conditions to the MDB and hence whether some characteristics of the drought were potentially predictable.

2 Methods

2.1 Linear Inverse Modeling

LIMs are a simple and computationally efficient method by which to emulate the observed stationary spatiotemporal statistics of a dynamical system (Penland and Matrosova, 1994). LIMs have been used extensively to understand observed climate variability, particularly its predictability (e.g., (Newman et al., 2016) for the Pacific Decadal Oscillation), and to produce seasonal and longer timescale forecasts (e.g., (Penland and Sardeshmukh, 1995) for ENSO). The predominant focus of LIMs in a climate context has been ENSO, with the associated LIMs trained on observed SSTs, and other fields like sea surface height and zonal surface winds that are critical for representing the state of the coupled atmosphere-ocean system in the tropical Pacific. Recently, however, LIMs have been constructed to also simulate climate fields that are driven by spatiotemporal variability in SSTs. In Ault et al. (2018), for instance, LIMs were used to produce a null hypothesis for the likelihood of persistent and severe droughts in southwestern North America. We closely follow this approach but instead focus on rainfall over Australia and its connection to the broader climate system (via SST anomalies).

2.2 Data

Monthly Australian rainfall data are from the Australian Gridded Climate Dataset v2 (AGCD), which is available at 0.05° latitude by 0.05° longitude resolution from 1900 to present (Evans et al., 2020). Across this time period, ~60-65 % of the MDB contains one or more physical rainfall monitoring stations per 0.25°; this fraction does not meaningfully change throughout our analysis period (Evans et al., 2020). Monthly sea surface temperature (SST) data are from two sources. SST data from 'Centennial in situ Observation-Based Estimates of the Variability of SST and Marine Meteorological Variables version 2' (COBE) are available at 1° latitude by 1° longitude resolution from 1891 to 2020 (Hirahara et al., 2014; Ishii et al., 2005). SST data from the US National Oceanic and Atmospheric Administration 'Extended Reconstruction SST version 5' (ERSST) are available at 2° latitude by 2° longitude resolution from 1854 to 2023 (Huang et al., 2017).

PREPRINT

2.2.1 Data processing

To construct LIMs describing Australian rainfall variability and the associated SST anomalies, we used 117 years of monthly gridded observational data (1900–2016). This is the full interval of overlap between the three datasets, excluding information from the 2017–2019 Tinderbox Drought. COBE and ERSST were regridded to a common 2.5° latitude by 2.5° longitude grid using bilinear interpolation and AGCD was regridded to 0.5° latitude by 0.5° longitude. In all cases the regridding decreases the nominal spatial resolution and helps to address computational and storage constraints. The data were then linearly detrended to minimize any influence of anthropogenic forcing, which is the only likely source of secular trends over the 1900-2016 interval. Further data processing specific to the LIM construction is described below in Section 2.3.

2.3 LIM construction

Our approach closely follows that of Ault et al. (2018) (see also Coats et al. (2020)). Here we focus on where the approaches differ. To quantify rainfall variability we use the AGCD. We excluded rainfall data from northern Australia, due to the highly non-linear nature of the monsoonal rainfall in this region (Fig. 1). To do this, we masked out the 'monsoonal north' and 'wet tropics' Australian natural resource management clusters, which in turn are based on logical areal groupings of long-term climatic conditions and biophysical factors (CSIRO and Bureau of Meteorology, 2015). We use both COBE and ERSST for the SST training data to test the sensitivity of our results to observational uncertainties. In both cases, we restricted the data to 55°S to 55°N, to minimize the influence of uncertainties in seasonal sea ice development on the SST field used for the LIMs (Huang et al., 2017). We subsequently refer to this dataset as 'global SST'.

LIMs are linear by construction and the training data is typically smoothed to remove weather, seasonal cycles, and other nonlinear variability. Following precedent (Ault et al., 2018; Coats et al., 2020), after removing the seasonal cycle over the full data period we then applied a three-month running mean. The 3-month running mean is also consistent with smoothing that is applied to Australian rainfall data in constructing drought metrics such as the Standardized Precipitation Index (e.g. Devanand et al., 2024).

LIMs are typically trained on a truncated space relative to the full data, utilizing a limited set of the expansion coefficients from an empirical orthogonal function (EOF) analysis. We retained the first 15 EOFs for SST (70% and 63% variance explained for COBE and ERSST, respectively) and the first 30 EOFs for rainfall (93% variance explained). As in Ault et al. (2018), the rainfall portion of the state

PREPRINT

vector was down-weighted by three orders of magnitude such that SSTs can impact rainfall in the LIMs but rainfall cannot impact SSTs. This down-weighting assumes that SST variability can drive Australian rainfall variability but not the other way around. All additional choices used to construct the LIMs are consistent with those in Ault et al. (2018); further details for producing and integrating the LIMs can be found therein.

We integrated each LIM (one each using COBE and ERSST training data) for 5000 years to produce covarying spatiotemporal trajectories of rainfall and SST that are consistent with the stationary linear lagged covariance statistics of the training datasets.

2.3.1 LIMs trained on SST variability in specific regions

To test the sensitivity of our results to SST variability in regions known to affect MDB rainfall, we additionally constructed LIMs trained on Australian rainfall data and SSTs in (a) only the tropical Pacific Ocean, or (b) only the Indian Ocean. The 'tropical Pacific Ocean' is defined as the Pacific Ocean from 20°S to 20°N. The Indian Ocean is defined as the Indian Ocean basin north of 55°S. Ocean boundaries are from the World Ocean Atlas (Garcia et al., 2019). We similarly retained the first 15 EOFs for SST (tropical Pacific Ocean: 95% and 96% variance explained for COBE and ERSST, respectively; Indian Ocean: 86% and 93% variance explained for COBE and ERSST, respectively).

2.4 Metrics of LIM performance

To test the skill of the LIMs in replicating the observed spatiotemporal statistics of the dynamical rainfall-SST system, we calculated the first two EOFs of the observed 1900–2016 global SST fields, processed as per Sections 2.2.1 and 2.3. We then calculated the correlations of the first two principal components of SST (PC1 and PC2) with Australian rainfall observations, similarly processed as per Sections 2.2.1 and 2.3. We repeated these steps using the LIM results, and calculated spatial correlations between each pair of grids (e.g., SST EOF1 in observations versus LIMs, using COBE as the SST training data). To calculate the spatial correlations for the pairs of two-dimensional grids, we flattened each grid, producing two directly comparable vectors, with each index position of each vector representing the values at a particular latitude-longitude pair.

We performed this analysis for all three sets of LIMs; that is, LIMs calculated using (a) global SSTs, (b) SSTs in the tropical Pacific Ocean, and (c) SSTs in the Indian Ocean. These comparisons provide estimates of how well the LIMs capture the dominant modes of variability in broad-scale SST variability and its connection to Australian rainfall.

2.5 Observational data treatment for comparison, encompassing the Tinderbox Drought

To directly compare rainfall anomalies during the drought with outputs of the LIMs, we applied all data processing steps (regridding, detrending and smoothing) described in Sections 2.2.1 and 2.3 to the same observational datasets, but extending to the end of 2019—thereby encompassing the drought. This enabled the observed drought and SST conditions during 2017–2019 to be directly compared to the LIMs results trained on the 1900–2016 datasets. Detrending by subtracting the 1900–2019 rather than 1900-2017 trend did not affect the results.

2.6 Quantifying MDB rainfall seasonality

The MDB spans different rainfall regimes, with a distinct north-south gradient in rainfall seasonality (Fig. 1). We quantified rainfall seasonality by subtracting the average percentage of annual rainfall that falls in the austral winter (JJA) from the average percentage of annual rainfall that falls in the austral summer (DJF). We calculated this metric for each grid cell in the AGCD, and used the results to divide the MDB into areas with summer-dominated rainfall (positive values) or winter-dominated rainfall (negative values).

2.7 Comparing observed and modelled anomalies

We calculated area-mean timeseries for rainfall over (a) the entire MDB, (b) the northern MDB, and (c) the southern MDB. The northern and southern MDB regions were defined based on their rainfall seasonality, as described in Section 2.6. To give equal area weighting when calculating area-mean rainfall, the gridded data were weighted by the square root of the cosine of latitude. We calculated the MDB area-mean rainfall timeseries for observations, as well as results from all LIMs.

We compared observed MDB rainfall anomalies during the 2017–2019 Tinderbox Drought with the distributions provided by the LIMs constructed using global SSTs. We did this for each individual drought year (2017, 2018, 2019), the two two-year sequences (2017–18, 2018–19), and the full three-year drought (2017–2019). We assessed both annual-total and austral cool-season (April to September) rainfall anomalies, because rainfall deficits during the drought were most anomalous in the cool season (Devanand et al., 2024). We also separately assessed anomalies over the sections of the MDB with summer-dominated rainfall (the northern MDB) versus winter-dominated rainfall (the southern MDB)

PREPRINT

(Fig. 1). In the results, we show whether observed rainfall anomalies during the Tinderbox Drought years were (a) exceeded in the 1900–2016 instrumental record; (b) unprecedented in the instrumental record but expected from the LIMs; or (c) unprecedented in the instrumental record *and* outside the range of the LIMs (suggesting an anthropogenic contribution or variability not sampled by the LIM).

2.7.1 Testing sensitivity of results to SST variability in particular regions

We repeated all analyses described in Section 2.7, but using distributions provided by the LIMs constructed using Australian rainfall and SSTs from only the tropical Pacific Ocean or only the Indian Ocean (as defined in Section 2.3.1).

2.8 SST anomalies during the driest years in the MDB

To identify SST anomaly patterns characteristically associated with dry conditions in the MDB, we identified—in the two 5000-year-long global ocean LIM outputs—the driest 5th percentile of years each in the MDB, the northern MDB and the southern MDB. That is, the 250 years with the most negative rainfall anomalies. We composited the annual mean SST and annual total Australian rainfall anomalies during those 250 years, and use stippling to show grid cells where >80% of the 250 years have an anomaly of the same sign (a positive SST/rainfall anomaly or a negative SST/rainfall anomaly). High agreement between the years suggests that this is likely to be an SST anomaly that promotes dry conditions in the MDB.

We also repeated this analysis using timeseries with a three-year running mean applied. This allowed us to identify the driest three-year periods in the MDB in each LIM output (that is, intervals of equal length to the Tinderbox Drought).

2.8.1 Relationship between dry years in the MDB and expected remote drivers of MDB rainfall variability

ENSO (Gillett et al., 2023; McBride and Nicholls, 1983; e.g. Risbey et al., 2009), the IOD (Ashok et al., 2003; McKay et al., 2023; e.g. Risbey et al., 2009), and SSTs in the ocean north of Australia (Nicholls, 2010; van Rensch et al., 2015) are all known remote drivers of MDB rainfall variability. We used the LIMs to assess long-term variability in how interactions between these drivers are related to dry years in the MDB, including during the Tinderbox Drought. We quantified ENSO using SST anomalies in the Niño 3.4 area (5°S to 5°N, 190°E to 240°E). We quantified IOD anomalies using the Dipole Mode Index (DMI), which is the gradient between the western (10°S to 10°N, 50°E to 70°E) and south-eastern (10°S

PREPRINT

to 0°, 90°E to 110°E) Indian Ocean SSTs. Following Nicholls (2010) and van Rensch et al. (2015), we also calculated area-mean SST anomalies in a box to the north of Australia (15°S to 0°, 110°E to 150°E).

For the 5000-year-long global ocean LIMs, we calculated annual mean values for each index. We show the full range of Niño 3.4, DMI, and northern Australian SST values, and highlight the values associated with the lowest fifth percentile of annual-total and cool-season rainfall (following Anderson et al., 2023). We compare these distributions with the Niño 3.4, DMI, and northern Australian SST values observed during each year of the Tinderbox Drought.

2.9 Characteristic rainfall anomalies when SST anomalies are most similar to the observed anomalies during the drought

We investigated whether the global SST anomalies observed during the three years of the Tinderbox Drought are expected to be associated with low rainfall over the MDB. Using the COBE and ERSST gridded datasets prepared as described in Section 2.5, we calculated annual mean SST anomaly maps for each year of the drought (2017, 2018, and 2019). We also calculated annual mean SST anomalies for each of the 5000-year-long LIM outputs, resulting in 5000 global anomaly maps for each SST product. We then used the Root Mean Squared (RMS) difference between the observations and each LIM year (cf. Ding et al., 2018) to identify the 10 years most closely matching SST anomalies observed during the drought. As in Section 2.8, we composited the annual mean SST anomalies and annual total Australian rainfall anomalies during those 10 years, and use stippling to show grid cells where eight or more of the 10 years have an anomaly of the same sign.

3 Results and discussion

3.1 Skill of LIMs in emulating the stationary statistics of Australian rainfall and its connection to global and regional SST anomalies

Figures S1–S3 demonstrate that the LIMs accurately capture observed variability in the rainfall-SST system. Broadly, correlations between Australian rainfall and SST PCs 1 and 2 are stronger in the LIMs than in observations. This is likely because the LIM represents the true system with a limited number of PCs for both SST and Australian rainfall and thus will contain less “noise” than the real world. That is, the truncated set of PCs used to represent the system means that the correlations—which are dominated by higher-order PCs—will tend to be accentuated.

PREPRINT

Results are highly consistent between LIMs constructed using SST data from COBE versus ERSST (Figs. S1–S3 a–h versus S1–S3 i–p), indicating a low sensitivity of our results to observational uncertainties. Therefore, when using the LIMs to produce distributions of possible anomalies in SST and Australian rainfall, we combine results from the two LIMs (resulting in distributions comprising 10,000 years of data).

In terms of spatial correlations between LIMs and observations across SST and its connection to Australian rainfall variability, LIMs constructed using SST data from ERSST perform very slightly better than LIMs constructed using COBE (Figs. S1–S3). Therefore, for the remainder of Section 3, when showing spatial patterns we show results from LIMs constructed using ERSST, and show the equivalent results from COBE in the Supplement.

3.2 How unusual was the Tinderbox Drought?

Considered as a three-year (2017–2019) rainfall deficit across the entire Murray-Darling Basin (MDB), the Tinderbox Drought was both historically unprecedented *and* beyond the range of rainfall anomalies produced by the LIMs (Fig. 2). This result is true for both annual and cool-season rainfall anomalies . The 3-year rainfall deficits were particularly large and exceptional in the northern MDB . In contrast, in the southern MDB the 3-year annual rainfall deficits were not the most extreme 3-year anomaly in the observational record, and the 3-year cool season rainfall deficits were historically unprecedented but not outside of expectation from the LIMs.

Of the three drought years, 2019 was the most extreme (orange points in Fig. 2), with 2018–2019 being the driest of the two-year sequences (brown points in Fig. 2). In the MDB, and more specifically in the northern MDB, 2018–2019 was outside of the expectation of the LIMs for both cool season and annual rainfall deficits. When considering 2019 alone, it was only the annual rainfall deficits in the northern MDB that were outside of the range of the LIMs. In contrast, the 2019 annual rainfall deficit over the full MDB and the 2019 cool-season rainfall deficit over the northern MDB were historically unprecedented in observational data but were within the range of the LIMs. Rainfall deficits in the southern MDB (across both seasons, and all combinations of years) were also within the range of possible anomalies produced by the LIMs, but were historically unprecedented in the instrumental record for the 2018–2019 annual total.

PREPRINT

Our LIM analysis suggests that it was the occurrence of three *sequential* dry years that made the Tinderbox Drought so exceptional (corroborating the findings of Devanand et al., 2024). In the case of 1, 2 and 3-year rainfall deficits that were historically unprecedented but fall within the LIM ranges (coloured squares in Fig. 2): based on the statistics of the instrumental record such rainfall deficits should be expected in the MDB, even though such extremes had not been historically experienced prior to the Tinderbox Drought. However, as the *full* 3-year drought did not fall within the LIM range, this suggests an anthropogenic contribution to the drought and/or variability that was not sampled by the LIMs (e.g., low frequency natural variability). This is particularly the case for cool-season rainfall over the northern MDB. Another way to say this is that although the individual years of the Tinderbox Drought were within the expected range of variability of MDB rainfall (over the entire basin), having sequential anomalies of the observed magnitude was not.

3.3 Influence of interbasin interactions on rainfall anomalies during the Tinderbox Drought

Exploration of the basin-specific LIMs suggests that interbasin interactions tend to limit drought severity in the MDB (Fig. S4). During the Tinderbox Drought, there were intervals with rainfall deficits that were unprecedented in the instrumental record and beyond the range of LIMs trained on global SSTs, but that are exceeded in LIMs where Australian rainfall variability is driven by only the tropical Pacific or Indian oceans (triangles in Fig. S4). For example, over the northern MDB the annual-total deficits observed in 2019, 2018–2019 and 2017–2019 were all outside of the LIM range based on global SSTs, but these observed anomalies are within the range of LIMs derived only from tropical Pacific SSTs. Similarly, despite being historically unprecedented and outside the LIMs trained on global SSTs, cool-season deficits over the entire MDB exceeding those observed in 2017–18, 2018–19, and 2017–2019 do occur in the Indian Ocean-only LIMs. Our findings indicate that more extreme rainfall deficits in the MDB occur in LIMs driven in isolation by the Indian or tropical Pacific oceans, but that drought extremes are reduced when both regions are included together as part of the global ocean.

As the LIMs do not include information about atmospheric circulation, in this study we are unable to diagnose the mechanisms driving these more extreme deficits. However, analysis of the impact of ENSO and the IOD on moisture delivery to Australia suggests that during co-occurring El Niño and positive IOD events (i.e., the ‘drying’ phases of both modes), a high pressure anomaly south of Australia results in a weak increase in moisture advected from the Tasman Sea to the MDB—slightly ameliorating the reduced moisture delivery from the south and west of Australia (Holgate et al., 2022). Further, climate model analyses suggest that Indian Ocean circulation changes can independently reduce rainfall over the

MDB via both a weaker Indian Walker Circulation—which inhibits convection, causing dry conditions—and weakening of the westerlies south of Australia, reducing the number of extratropical lows and frontal systems reaching southern Australia (Taschetto et al., 2011; Ummenhofer et al., 2009). Even with the more extreme range of drought conditions produced by LIMs driven only by the Indian or tropical Pacific oceans, the 3-year sequential rainfall deficits of the Tinderbox Drought remain outside of the all-LIMs range for the 2017–2019 cool season rainfall deficits in the northern MDB. This also holds for the 2-year cool season deficits over the northern MDB in 2017–2018 and 2018–2019. This further strengthens our findings that it was the cool-season rainfall deficits over the northern MDB, and the 3-year sequence of these deficits, that were the most exceptional characteristics of rainfall deficits during the Tinderbox Drought.

3.4 Global SST anomalies promoting low rainfall over the MDB

The LIMs suggest that the most consistent predictors of dry years in the MDB are warmer-than-average SSTs across the central to eastern tropical Pacific Ocean and the western Indian Ocean (Fig. 3, Fig. S5). This is the case for both single years and three-year mean rainfall deficits (not shown), and the full MDB as well as the northern and southern MDB. Cool SST anomalies in the Tasman and Coral Seas are also consistent predictors of dry years in the LIMs constructed using SST data from COBE, particularly for the northern MDB (Fig. S5). The associated SST anomaly pattern is reminiscent of global SST anomalies during simultaneous El Niño and positive IOD conditions, and the association of dry MDB years with these phases of tropical Indo-Pacific variability is clear in Fig. 4.

Despite the persistent association of dry anomalies in the MDB with tropical Indo-Pacific SST variability, the extreme rainfall deficits of the Tinderbox Drought did not correspond to this expected SST relationship (Figs. 4–5). During the Tinderbox Drought, only the final (and driest) year of the drought was associated with a weak central-Pacific El Niño event as well as an extreme positive IOD event (Figs. 4–5, Fig. S6). This positive IOD event was well beyond the range of the LIMs (Fig. 4)—particularly in its lack of association with a large positive Niño 3.4 SST anomaly. For comparison, the second-strongest positive IOD event on record, in 1997, was associated with an extreme El Niño event, as would be expected from Figure 4. We note that it is possible that the relatively coarse grid resolution of the LIMs fails to accurately capture and model the full extent of Indian Ocean SST variability. Nevertheless, our findings suggest that an anthropogenic influence on global SST variability contributed to the occurrence of an extreme positive IOD event in the absence of a strong tropical Pacific SST anomaly, which in turn drove very low rainfall across the MDB. Additionally, the occurrence of an

PREPRINT

unprecedentedly strong positive IOD event is consistent with paleoclimate, historical and climate model evidence which all indicate that positive IOD events will become more frequent and more extreme in a warming world, along with decreased strength of coupling to tropical Pacific SSTs (Abram et al., 2020; Ham et al., 2017).

Previous work has also highlighted the importance of SST anomalies to the north of Australia in predicting dry years in the MDB (Devanand et al., 2024; Nicholls, 2010; van Rensch et al., 2015). Single dry years in the MDB LIMs are associated with co-occurring positive anomalies in the Niño 3.4 region and cooler-than-average SSTs to the north of Australia (Fig. 3, Fig. S5, Fig. S7). However, cool SSTs to the north of Australia are not as reliable a predictor of dry conditions over the MDB as a positive IOD (Fig. 4 compared with Fig. S7). Nevertheless, the driest year of the Tinderbox Drought (2019) fell within the range of coinciding Niño 3.4 and northern Australian SST anomalies that are expected to bring dry conditions to the MDB (Fig. S7). We also note that this result differs slightly from Devanand et al. (2024), who found that northern Australian SST anomalies were negative on average across April to September of each year of the Tinderbox Drought. However, Devanand et al. (2024) used a different region to define 'northern Australian SST', which specifically targeted the area of strongest correlations between SST and their drought focus region, and extends further south and east than the region defined by Nicholls (2010).

3.5 Do SST anomalies observed during the Tinderbox Drought reliably bring dry conditions to the MDB?

The LIMs can also be used to find analogue SST patterns that are most consistent with the observed SST anomalies during each year of the Tinderbox Drought (Fig. 5 and Fig. S6). The annual mean SST anomaly pattern observed during the first year of the drought is not reliably associated with a dry MDB (Fig. 5 and Fig. S6, first column), and for the second year only the LIMs constructed with COBE are associated with dry MDB conditions (Fig. 5 and Fig. S6, second column). SST anomalies during the final year of the drought are reliably associated with dry conditions across much of the MDB (Fig. 5 and Fig. S6, third column), although the areas with consistent dry anomalies differ slightly between the two models. The ERSST-based LIMs show consistent dry anomalies in the southern and central MDB (Fig. 5) whereas the COBE-based LIMs show dry anomalies in the northern MDB, extending across central Australia (Fig. S6). Together, these results suggest that the rainfall deficits experienced during the Tinderbox Drought were not the most likely outcome given the global SST anomaly pattern.

3.6 Implications

Our findings indicate that the observed rainfall deficits during the Tinderbox Drought, and specifically the 3-year sequence of these anomalies, were worse than could have been expected based on the historical association of Australian rainfall and global SST variability. The multi-millennial length of the LIMs provides enough realisations of possible rainfall sequences to rule out this 3-year drought as simply being a manifestation of natural climate variability on timescales up to multi-decadal. Instead, our findings suggest that other factors beyond SST variability contributed to the Tinderbox Drought being worse than could have been anticipated. This is reinforced by findings that the tropical Indo-Pacific SST conditions during the Tinderbox Drought did not follow the expected behaviour that has historically been associated with dry conditions in the MDB, and that LIM analogues of the observed global SST patterns during the drought years are not reliably associated with dry conditions in the MDB, and can not account for the extreme intensity and northern MDB focus of the observed rainfall deficits.

The Tinderbox Drought was likely worsened by processes not represented in the statistical LIMs, including human-caused climate change. Key characteristics of this drought included that it was hotter than it would have been without human-caused climate warming, and that associated rising vapour pressure deficit made the atmosphere thirstier than it would have been for analogous droughts without the influence of climate change (Devanand et al., 2024). While equivocal attribution of observed rainfall trends over the MDB is not yet possible, there has been an observed decrease in cool season rainfall and an increased number of below average rainfall years in southeast Australia (BoM, 2022). These rainfall trends are not incorporated in our LIMs, and climate model analyses suggest that human-caused climate change worsened the cool-season rainfall deficits of the Tinderbox Drought by around 18% (Devanand et al., 2024).

Other atmospheric variability processes that are unaffected by SST variability were also a characteristic of the Tinderbox Drought. The final and most intense year of the drought included a rare sudden stratospheric warming event over Antarctica which is associated with intense dry conditions and increased fire risk over the northern MDB (Lim et al., 2019). In particular, this may have intensified the northern MDB component of rainfall deficits which were found to be particularly exceptional in our LIMs analysis, and acted in conjunction with the very strong positive IOD event that developed in the same year and is more typically associated with rainfall deficits in the southern MDB.

PREPRINT

Numerous aspects of continued human-caused climate change are expected to make it even more likely that intense drought conditions will be experienced in the MDB that are beyond historical experience and also beyond the range of what could have been anticipated from natural variability without climate change. Rainfall in the MDB is projected to decline this century, particularly in the cool-season (Grose et al., 2020). Future droughts will also be hotter than the equivalent drought would have been in a world without human-caused climate warming, and associated increases in vapour pressure deficit will enhance the ability for the land surface to dry. This drying provides a feedback that further reduces locally-derived rainfall during drought periods (e.g., Devanand et al., 2024). Noting that most MDB runoff is generated across the southeastern MDB during the cool season (Potter et al., 2010; Donohue et al., 2011), future reductions in cool season rainfall will have implications for water management in the MDB—including, for example, determining the balance between consumptive water use and water for the environment (Prosser et al., 2021). This will be the case even during droughts similar to the Tinderbox Drought, where deficits were more focused in the northern MDB. Therefore, a possible future application of our LIM approach is to use the model outputs as the basis for a wider range of stochastic MDB flow scenarios when determining water management plans (following the suggestion of Prosser et al., 2021).

Human-caused climate change is also expected to increase the frequency and severity of positive IOD events (e.g., Abram et al., 2020; Wang et al., 2024), increasing the chance of rainfall impacts that are beyond the range that could be anticipated from historical experience using the LIMs framework. Together our findings suggest that the Tinderbox Drought may be an indication of the type of unexpectedly extreme events that Australia will need to build resilience to, even in the absence of being able to fully anticipate the potential intensity of these extreme events.

3.7 Limitations of Linear Inverse Models for assessing drought characteristics

The LIM approach is a powerful tool for assessing the 'unusualness' of a multi-year extreme rainfall event such as the Tinderbox Drought, given climate models have known biases in Australian rainfall, and the relevant Australian paleoclimate proxy record is sparse. The two major drawbacks of using an observations-based statistical framework to assess the Tinderbox Drought are that: 1) all rainfall and SST observations used to construct the models were taken within a time when human activities were already affecting the climate; and 2) low frequency (multi-decadal and longer timescale) variability is not well sampled by the LIMs. Hence, future studies analyzing modern extreme hydroclimate events in the context of natural variability should also seek to obtain information from annually-resolved, local hydroclimate proxy records with a strong mechanistic relationship to MDB rainfall. That is, proxies for which we thoroughly understand the processes that encode a hydroclimate signal in a natural archive (e.g., tree wood, stalagmite, or lake sediment), and can hence compare directly with observed events.

4 Conclusions

Rainfall deficits during Australia's 2017–2019 Tinderbox Drought were beyond expectations based on rainfall variability during the preceding century. Rainfall deficits were largest in the northern MDB (which has summer-dominated rainfall), and in the cool season (from April to September). The occurrence of unprecedented rainfall deficits during the Tinderbox Drought—beyond the range from the LIMs—suggests a contribution of anthropogenic climate change or out-of-sample climate variability (e.g., low-frequency variability) to the overall severity of the drought. The relationship between Australian rainfall and global SSTs suggests that the most reliable predictors of rainfall deficits over the MDB are co-occurring El Niño and positive IOD conditions. This is the case for both annual-total and cool season rainfall, however, these conditions were not present throughout the Tinderbox Drought. Of particular note was an extreme positive IOD event, well outside the range of the LIMs, that likely contributed to deficits during 2019 which was the driest year of the drought. The occurrence of this exceptionally severe drought—that was not predictable based on all previous rainfall observations—suggests that anthropogenic climate change may result in more unprecedented drought events in the future.

Acknowledgements

This work was supported by the Australian Research Council Centre of Excellence for Climate Extremes (CE170100023). We also acknowledge support from the National Computational Infrastructure (NCI), which is supported by the Australian Government.

Author contributions

GF conceptualised the study and created all figures. SC constructed the LIMs. GF and SC developed the methodology, performed all formal analysis, and wrote the manuscript. All authors contributed to manuscript editing and review.

Data availability

All data used in this work are publicly available. The Australian Gridded Climate Dataset v2 (AGCD) is accessible from the Australian National Computational Infrastructure at https://dx.doi.org/10.25914/6009600786063 (BoM, 2020). SST data from COBE are available to

PREPRINT

download from https://ds.data.jma.go.jp/tcc/tcc/products/elnino/cobesst_doc.html. SST data from ERSST are available to download from https://psl.noaa.gov/data/gridded/data.noaa.ersst.v5.html.

All LIM outputs produced for this work will be made publicly available in a Zenodo repository at the time of publication.

References

Abram, N.J., Hargreaves, J.A., Wright, N.M., Thirumalai, K., Ummenhofer, C.C., England, M.H., 2020. Palaeoclimate perspectives on the Indian Ocean Dipole. Quat. Sci. Rev. 237, 106302. https://doi.org/10.1016/j.quascirev.2020.106302

Anderson, T.G., McKinnon, K.A., Pons, D., Anchukaitis, K.J., 2023. How exceptional was the 2015–2019 central American drought? Geophys. Res. Lett. 50. https://doi.org/10.1029/2023gl105391

Ashok, K., Guan, Z., Yamagata, T., 2003. Influence of the Indian Ocean Dipole on the Australian winter rainfall. Geophys. Res. Lett.

Ault, T.R., St. George, S., Smerdon, J.E., Coats, S., Mankin, J.S., Carrillo, C.M., Cook, B.I., Stevenson, S., 2018. A Robust Null Hypothesis for the Potential Causes of Megadrought in Western North America. J. Clim. 31, 3–24. https://doi.org/10.1175/JCLI-D-17-0154.1

Australian Bureau of Meteorology (BoM), 2020. Australian Gridded Climate Data (AGCD) v2.0.0" Downloaded from https://dx.doi.org/10.25914/6009600786063 in September 2023.

Australian Bureau of Meteorology (BoM), 2022. State of the Climate 2022. Commonwealth of Australia. Available from http://www.bom.gov.au/state-of-the-climate/

Coats, S., Smerdon, J.E., Stevenson, S., Fasullo, J.T., Otto-Bliesner, B., Ault, T.R., 2020. Paleoclimate Constraints on the Spatiotemporal Character of Past and Future Droughts. J. Clim. 33, 9883–9903. https://doi.org/10.1175/JCLI-D-20-0004.1

Cook, B.I., Palmer, J.G., Cook, E.R., Turney, C.S.M., Allen, K., Fenwick, P., O'Donnell, A., Lough, J.M., Grierson, P.F., Ho, M., Baker, P.J., 2016. The paleoclimate context and future trajectory of extreme summer hydroclimate in eastern Australia. J. Geophys. Res. D: Atmos. 121, 12,820–12,838. https://doi.org/10.1002/2016JD024892

CSIRO and Bureau of Meteorology, 2015. Climate Change in Australia Information for Australia's Natural Resource Management Regions: Technical Report. CSIRO and Bureau of Meteorology, Australia.

PREPRINT

Devanand, A., Falster, G.M., Gillett, Z.E., Hobeichi, S., Holgate, C.M., Jin, C., Mu, M., Parker, T., Rifai, S.W., Rome, K.S., Stojanovic, M., Vogel, E., Abram, N.J., Abramowitz, G., Coats, S., Evans, J.P., Gallant, A.J.E., Pitman, A.J., Power, S.B., Rauniyar, S.P., Taschetto, A.S., Ukkola, A.M., 2024. Australia's Tinderbox Drought: An extreme natural event likely worsened by human-caused climate change. Sci Adv 10, eadj3460. https://doi.org/10.1126/sciadv.adj3460

Ding, H., M. Newman, M. A. Alexander, and A. T. Wittenberg, 2018. Skillful Climate Forecasts of the Tropical Indo-Pacific Ocean Using Model-Analogs. J. Climate, 31, 5437–5459, https://doi.org/10.1175/JCLI-D-17-0661.1.

Donohue, R. J., Roderick, M. L., McVicar, T. R, 2011. Assessing the differences in sensitivities of runoff to changes in climatic conditions across a large basin, Journal of Hydrology 406(3–4), 234-244, https://doi.org/10.1016/j.jhydrol.2011.07.003.

Evans, A., Jones, D., Lellyett, S., Smalley, R., 2020. An Enhanced Gridded Rainfall Analysis Scheme for Australia. Australian Bureau of Meteorology.

Falster, G.M., Wright, N.M., Abram, N.J., Ukkola, A.M., Henley, B.J., 2024. Potential for historically unprecedented Australian droughts from natural variability and climate change. Hydrol. Earth Syst. Sci. 28, 1383–1401. https://doi.org/10.5194/hess-28-1383-2024

Freund, M., Henley, B., Karoly, D., Allen, K., 2017. Multi-century cool-and warm-season rainfall reconstructions for Australia's major climatic regions. Climate of the Past.

Garcia H.E., Boyer, T. P., Baranova, O.K., Locarnini, R.A., Mishonov, A.V, Grodsky, A, Paver, C.R, Weathers, K.W, Smolyar, I.V., Reagan, J.R., Seidov, D., Zweng, M. M., 2019. World Ocean Atlas 2018: Product Documentation. A. Mishonov, Technical Editor

Gillett, Z.E., Taschetto, A.S., Holgate, C.M., Santoso, A., 2023. Linking ENSO to synoptic weather systems in eastern Australia. Geophys. Res. Lett. 50. https://doi.org/10.1029/2023gl104814

Grose, M.R., Narsey, S., Delage, F.P., Dowdy, A.J., Bador, M., Boschat, G., Chung, C., Kajtar, J.B., Rauniyar, S., Freund, M.B., Lyu, K., Rashid, H., Zhang, X., Wales, S., Trenham, C., Holbrook, N.J., Cowan, T., Alexander, L., Arblaster, J.M., Power, S., 2020. Insights from CMIP6 for Australia's future climate. Earths Future 8, e2019EF001469. https://doi.org/10.1029/2019ef001469

Ham, Y.-G., Choi, J.-Y., Kug, J.-S., 2017. The weakening of the ENSO–Indian Ocean Dipole (IOD) coupling strength in recent decades. Clim. Dyn. 49, 249–261. https://doi.org/10.1007/s00382-016-3339-5

Hirahara, S., Ishii, M., Fukuda, Y., 2014. Centennial-Scale Sea Surface Temperature Analysis and Its Uncertainty. J. Clim. 27, 57–75. https://doi.org/10.1175/JCLI-D-12-00837.1

PREPRINT

Ho, M., Kiem, A.S., Verdon-Kidd, D.C., 2015. A paleoclimate rainfall reconstruction in the Murray-Darling Basin (MDB), Australia: 2. Assessing hydroclimatic risk using paleoclimate records of wet and dry epochs. Water Resour. Res. 51, 8380–8396. https://doi.org/10.1002/2015wr017059

Holgate, C., J. P. Evans, A. S. Taschetto, A. S. Gupta, and A. Santoso, 2022: The Impact of Interacting Climate Modes on East Australian Precipitation Moisture Sources. J. Climate, 35, 3147–3159, https://doi.org/10.1175/JCLI-D-21-0750.1.

Huang, B., Thorne, P.W., Banzon, V.F., Boyer, T., Chepurin, G., Lawrimore, J.H., Menne, M.J., Smith, T.M., Vose, R.S., Zhang, H.-M., 2017. Extended Reconstructed Sea Surface Temperature, Version 5 (ERSSTv5): Upgrades, Validations, and Intercomparisons. J. Clim. 30, 8179–8205. https://doi.org/10.1175/JCLI-D-16-0836.1

Ishii, M., Shouji, A., Sugimoto, S., Matsumoto, T., 2005. Objective analyses of sea-surface temperature and marine meteorological variables for the 20th century using ICOADS and the Kobe Collection. Int. J. Climatol. 25, 865–879. https://doi.org/10.1002/joc.1169

King, A.D., Donat, M.G., Alexander, L.V., Karoly, D. J., 2015. The ENSO-Australian rainfall teleconnection in reanalysis and CMIP5. Clim Dyn 44, 2623–2635. https://doi.org/10.1007/s00382-014-2159-8.

Lansbury, N., Moggridge, B., Creamer, S., Ireland, L., Buckley, L., Evans, G., Milsom, O., Pecl, G., Mosby, V., 2023. Aboriginal and Torres Strait Islander Peoples' voices and emgagement in the Intergovernmental Panel on Climate Change: Advice to inform the Australian Government towards Assessment Report 7. Independent report to the Australia Government, available from https://public-health.uq.edu.au/files/25162/IPCC-Voices-Report.pdf.

Lim, E.-P., Hendon, H.H., Boschat, G., Hudson, D., Thompson, D.W.J., Dowdy, A.J., Arblaster, J.M., 2019. Australian hot and dry extremes induced by weakenings of the stratospheric polar vortex. Nat. Geosci. 12, 896–901. https://doi.org/10.1038/s41561-019-0456-x

Mankin, J.S., Lehner, F., Coats, S., McKinnon, K.A., 2020. The value of initial condition large ensembles to robust adaptation decision-making. Earths Future 8. https://doi.org/10.1029/2020ef001610

McBride, J.L., Nicholls, N., 1983. Seasonal Relationships between Australian Rainfall and the Southern Oscillation. Mon. Weather Rev. 111, 1998–2004. https://doi.org/10.1175/1520-0493(1983)111<1998:SRBARA>2.0.CO;2

McKay, R.C., Boschat, G., Rudeva, I., Pepler, A., Purich, A., Dowdy, A., Hope, P., Gillett, Z.E., Rauniyar, S., 2023. Can southern Australian rainfall decline be explained? A review of possible drivers. Wiley Interdiscip. Rev. Clim. Change 14. https://doi.org/10.1002/wcc.820

Newman, M., Alexander, M.A., Ault, T.R., Cobb, K.M., Deser, C., Di Lorenzo, E., Mantua, N.J., Miller, A.J., Minobe, S.,

PREPRINT

Nakamura, H., Schneider, N., Vimont, D.J., Phillips, A.S., Scott, J.D., Smith, C.A., 2016. The Pacific Decadal Oscillation, Revisited. J. Clim. 29, 4399–4427. https://doi.org/10.1175/JCLI-D-15-0508.1

Nicholls, N., 2010. Local and remote causes of the southern Australian autumn-winter rainfall decline, 1958–2007. Clim. Dyn. 34, 835–845. https://doi.org/10.1007/s00382-009-0527-6

Palmer, J.G., Verdon-Kidd, D., Allen, K.J., Higgins, P., Cook, B.I., Cook, E.R., Turney, C.S.M., Baker, P.J., 2023. Drought and deluge: the recurrence of hydroclimate extremes during the past 600 years in eastern Australia's Natural Resource Management (NRM) clusters. Nat. Hazards. https://doi.org/10.1007/s11069-023-06288-0

Penland, C., Matrosova, L., 1994. A Balance Condition for Stochastic Numerical Models with Application to the El Niño-Southern Oscillation. J. Clim. 7, 1352–1372. https://doi.org/10.1175/1520-0442(1994)007<1352:ABCFSN>2.0.CO;2

Penland, C., Sardeshmukh, P.D., 1995. The Optimal Growth of Tropical Sea Surface Temperature Anomalies. J. Clim. 8, 1999–2024. https://doi.org/10.1175/1520-0442(1995)008<1999:TOGOTS>2.0.CO;2

Potter, N. J, Chiew, F. H. S., Frost, A. J., 2010. An assessment of the severity of recent reductions in rainfall and runoff in the Murray–Darling Basin, Journal of Hydrology 381(1–2), 52-64, https://doi.org/10.1016/j.jhydrol.2009.11.025

Risbey, J.S., Pook, M.J., McIntosh, P.C., Wheeler, M.C., Hendon, H.H., 2009. On the Remote Drivers of Rainfall Variability in Australia. Mon. Weather Rev. 137, 3233–3253. https://doi.org/10.1175/2009MWR2861.1

Stewart, I. T., Rogers, J., Graham, A., 2020. Water security under severe drought and climate change: Disparate impacts of the recent severe drought on environmental flows and water supplies in Central California. Journal of Hydrology X 7, 100054. https://doi.org/10.1016/j.hydroa.2020.100054.

Taschetto, A. S., A. Sen Gupta, H. H. Hendon, C. C. Ummenhofer, and M. H. England, 2011. The Contribution of Indian Ocean Sea Surface Temperature Anomalies on Australian Summer Rainfall during El Niño Events. J. Climate, 24, 3734–3747, https://doi.org/10.1175/2011JCLI3885.1.

Ummenhofer, C. C., A. Sen Gupta, A. S. Taschetto, and M. H. England, 2009: Modulation of Australian Precipitation by Meridional Gradients in East Indian Ocean Sea Surface Temperature. J. Climate, 22, 5597-5610, https://doi.org/10.1175/2009JCLI3021.1.

Vance, T.R., Roberts, J.L., Plummer, C.T., Kiem, A.S., van Ommen, T.D., 2015. Interdecadal Pacific variability and eastern Australian megadroughts over the last millennium. Geophys. Res. Lett. 42, 129–137. https://doi.org/10.1002/2014gl062447

van Rensch, P., Gallant, A.J.E., Cai, W., Nicholls, N., 2015. Evidence of local sea surface temperatures overriding the

PREPRINT

southeast Australian rainfall response to the 1997–1998 El Niño. Geophys. Res. Lett. 42, 9449–9456. https://doi.org/10.1002/2015gl066319

Vertessy, R., Barma, D., Baumgartner, L., Mitrovic, S., Sheldon, F., Bond, N., 2019. Independent assessment of the 2018-19 fish deaths in the lower Darling. Independent report for the Australian Government Murray-Darling Basin Authority. Available online from https://www.mdba.gov.au/publications-and-data/publications/response-fish-deaths-lower-darling

Wang, G., Cai, W., Santoso, A.. Abram, N., Ng, B., Yang, K., Geng, T., Doi, T., Du, Y., Izumo, T., Ashok, K., Li, J., Li, T., McKenna, S., Sun, S., Tozuka, T., Zheng, X., Liu, Y., Wu, L., Jia, F., Hu, S., Li., X., 2024.. The Indian Ocean Dipole in a warming world. Nat Rev Earth Environ 5, 588–604. https://doi.org/10.1038/s43017-024-00573-7

Wittwer, G., Waschik, R., 2021. Estimating the economic impacts of the 2017–2019 drought and 2019–2020 bushfires on regional NSW and the rest of Australia. Aust. J. Agric. Resour. Econ. 65, 918–936. https://doi.org/10.1111/1467-8489.12441

Wood, R.R., Lehner, F., Pendergrass, A.G., Schlunegger, S., 2021. Changes in precipitation variability across time scales in multiple global climate model large ensembles. Environ. Res. Lett. 16, 084022. https://doi.org/10.1088/1748-9326/ac10dd

PREPRINT

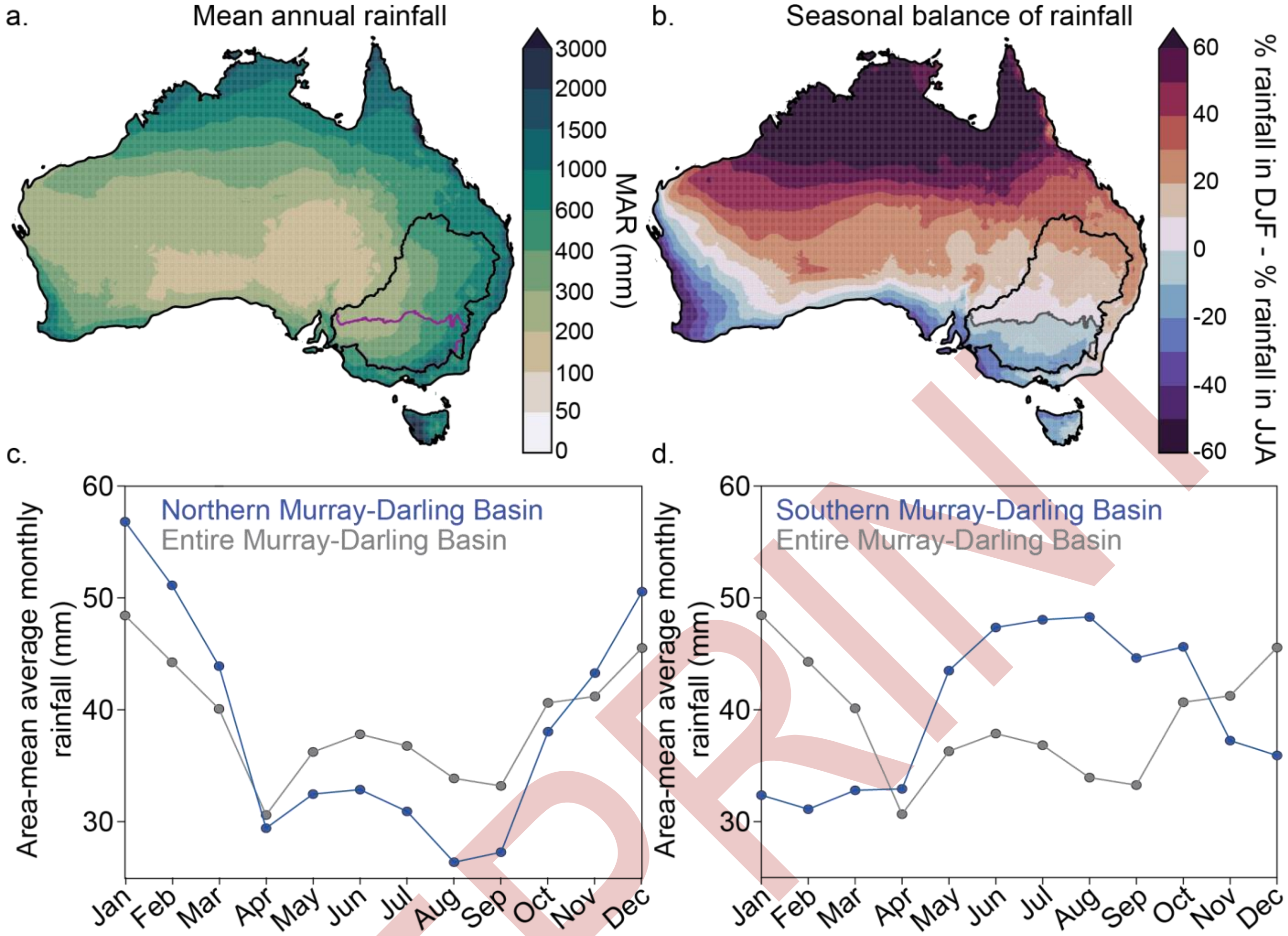

Fig. 1. Long-term (1900-2019) rainfall statistics for Australia, using data from the AGCD. a) Mean annual rainfall. b) Average seasonal balance of rainfall, calculated as the percentage of annual total rainfall that falls in DJF minus the percentage of annual total rainfall that falls in JJA. In areas with red-toned colours, most rainfall is delivered in the austral summer (DJF). In areas with blue-toned colours, most rainfall is delivered in the austral winter (JJA). Black outline in panels a) and b) shows the Murray-Darling Basin (MDB); purple (panel a) or grey (panel b) line inside the MDB shows the boundary between summer-dominated rainfall (the northern MDB) and winter-dominated rainfall (the southern MDB). c) Area-mean long-term average (1900-2019) seasonal cycle of rainfall in the northern MDB (blue line) compared with the area-mean seasonal cycle of rainfall across the entire MDB (grey line). d) Area-mean long-term average seasonal cycle of rainfall in the southern MDB (blue line) compared with the area-mean seasonal cycle of rainfall across the entire MDB (grey line).

PREPRINT

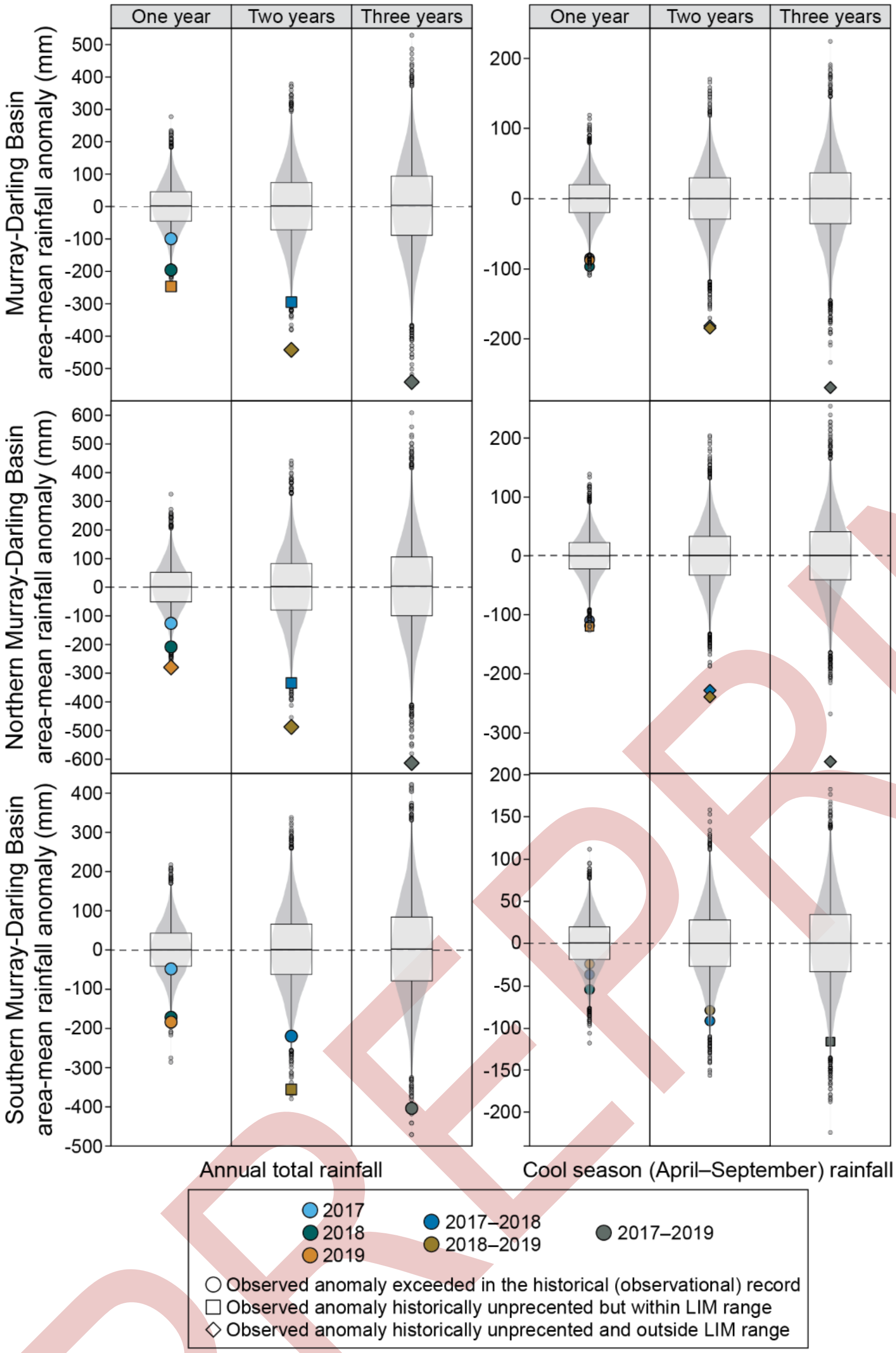

Fig. 2. Violin-and-boxplots ('voxplots') showing where MDB rainfall anomalies observed during the Tinderbox Drought fall relative to the full range of MDB rainfall anomalies in LIMs trained on global SSTs. Anomalies are shown in terms of single year anomalies, anomalies over two consecutive years, and anomalies over three consecutive years. Left column shows anomalies in annual total rainfall, right column shows anomalies in cool-season (April to September) rainfall. First row shows anomalies in area-mean rainfall over the entire MDB, second row shows anomalies in area-mean rainfall over the northern MDB (summer-dominated rainfall regime; Fig. 1b,c); third row shows anomalies in area-mean rainfall over the southern MDB (winter-dominated rainfall regime; Fig. 1b,d). Voxplots show full distribution of values from the LIMs. Coloured shapes show anomalies observed during the Tinderbox Drought. Points showing observed anomalies are shaped according to whether the anomaly was exceeded in the 1900–2016 instrumental record (circle), unprecedented in the instrumental record but expected

from the LIMs (square), or unprecedented in the instrumental record *and* outside the range of the LIMs (suggesting an anthropogenic contribution or variability not sampled by the LIM; diamond).

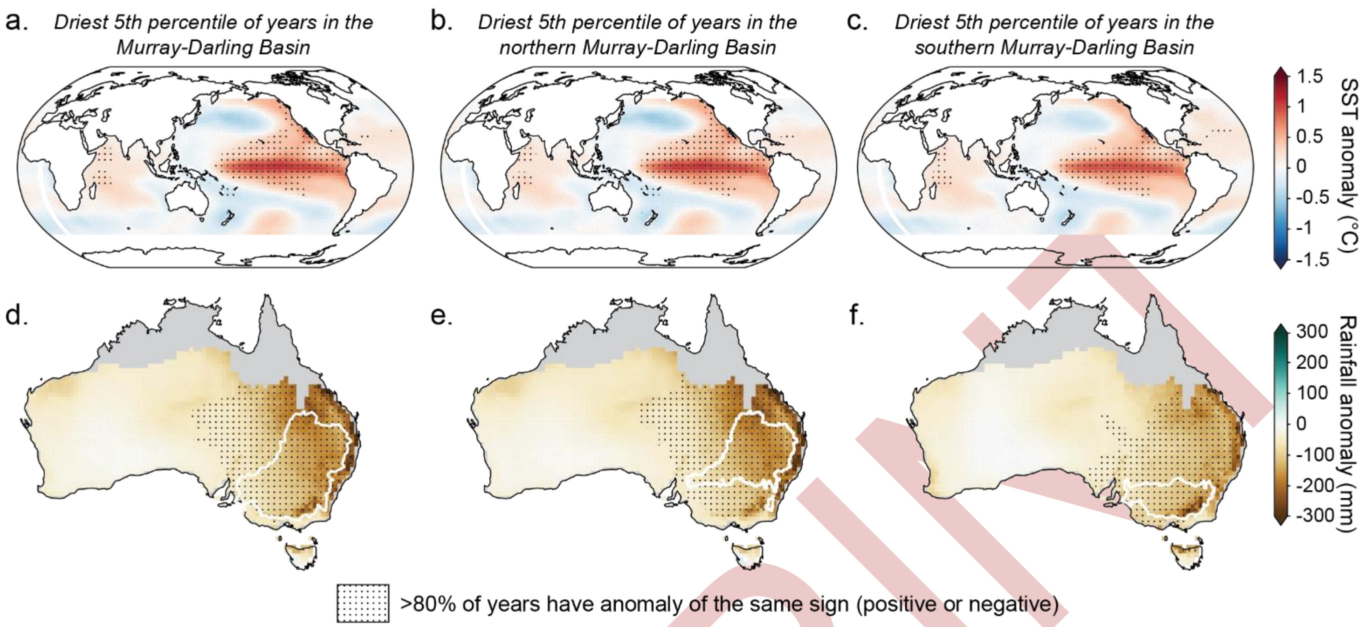

Fig. 3. Maps showing SST and rainfall anomalies during the driest 5th percentile of years in the MDB (in terms of annual total rainfall), in LIMs constructed using global SST data from ERSST. (a) Mean SST anomalies during the driest 5th percentile of years in the MDB (b) Mean SST anomalies during the driest 5th percentile of years in the northern MDB. (c) Mean SST anomalies during the driest 5th percentile of years in the southern MDB. (d) Mean total annual Australian rainfall anomalies during the driest 5th percentile of years in the MDB (e) Mean total annual Australian rainfall anomalies during the driest 5th percentile of years in the northern MDB. (f) Mean total annual Australian rainfall anomalies during the driest 5th percentile of years in the southern MDB. Stippling shows cells where >80% of years have an anomaly of the same sign. Figure is based on annual total rainfall, but similar results are seen for cool seasonal rainfall (not shown).

PREPRINT

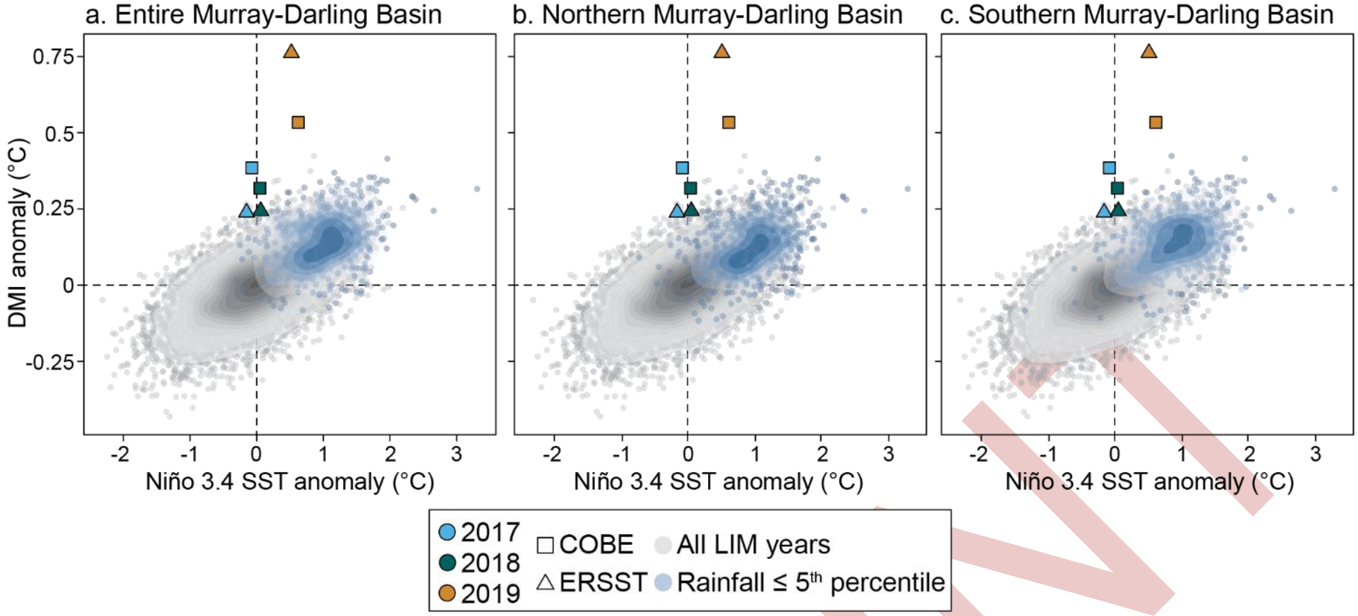

Fig. 4. Cross-plots showing co-occurring Niño 3.4 SST and Dipole Mode Index (DMI) anomalies in the LIMs constructed using global SSTs. Grey points and density shading show values for all 10,000 LIM years. Blue points and density shading show years when annual total MDB rainfall is in the lowest 5th percentile. Coloured points show Niño 3.4 SST and DMI anomalies observed during each year of the Tinderbox Drought. Squares denote SST observations from COBE; triangles denote SST observations from ERSST. (a) highlighting years where rainfall over the entire MDB is in the lowest 5th percentile. (b) highlighting years where rainfall over the northern MDB is in the lowest 5th percentile. (c) highlighting yea rs where rainfall over the southern MDB is in the lowest 5th percentile. Note that results are very similar for both cool season rainfall, and rainfall anomalies calculated as three-year totals (i.e., the length of the Tinderbox Drought).

PREPRINT

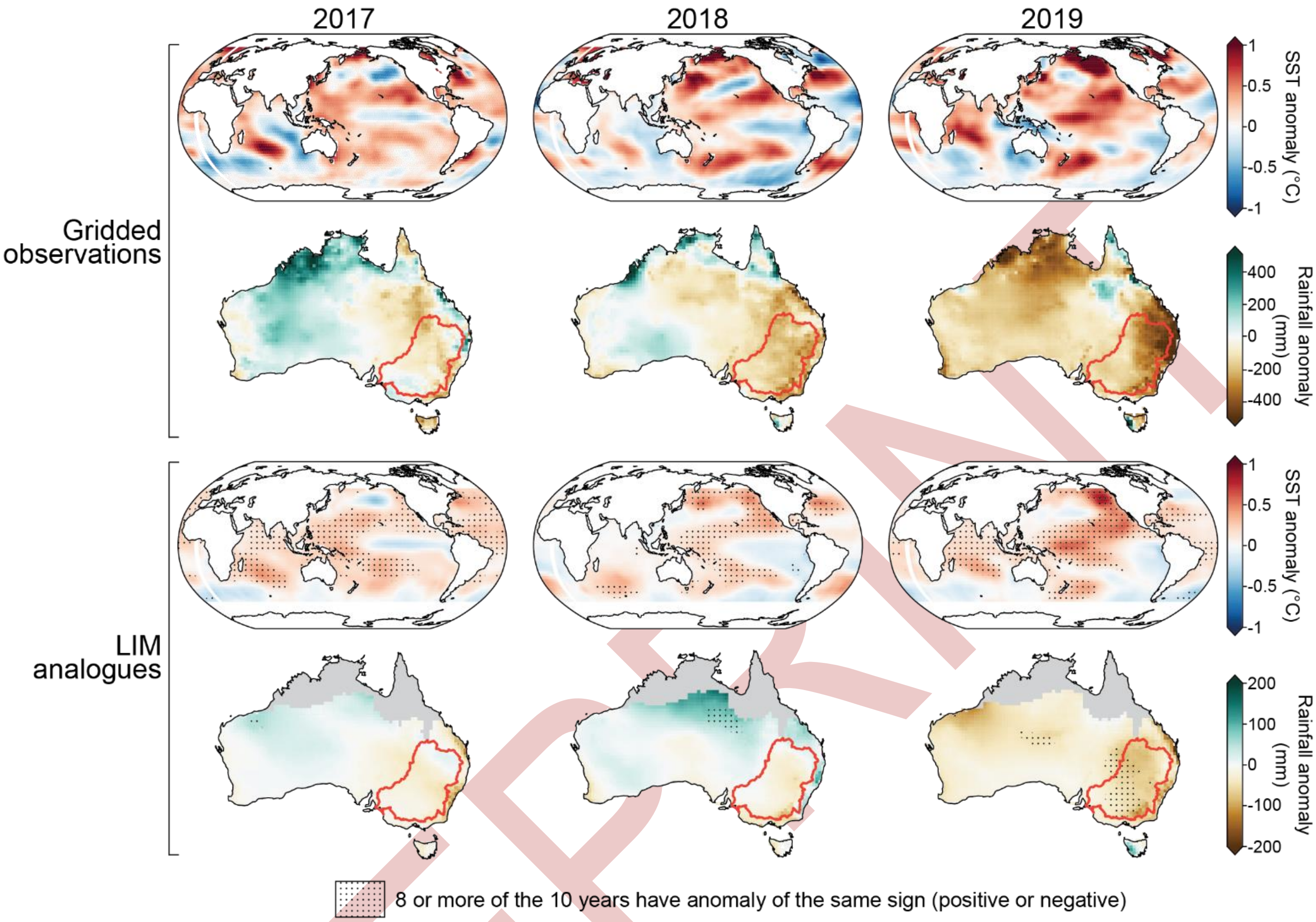

Fig. 5. Maps showing annual mean SST and annual total rainfall anomalies observed during each year of the Tinderbox Drought (top two rows), and analogues in LIMs constructed using global SST data from ERSST (bottom two rows). Top row shows observed annual mean SST anomalies during each year of the Tinderbox Drought (2017, 2018, 2019), in ERSST. Second row shows observed annual total Australian rainfall anomalies during each year of the drought, in the AGCD. Third row shows the average SST anomalies for the ten LIM years most similar to those shown in the top row, determined using the RMS difference. Bottom row shows average Australian rainfall anomalies in those same ten LIM years. Stippling in the bottom two rows shows cells where eight or more of the 10 years have an anomaly of the same sign.

PREPRINT